Brain Research Bulletin 212 (2024) 110938

Contents lists available at ScienceDirect

Brain Research Bulletin

journal homepage: www.elsevier.com/locate/brainresbull

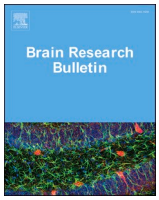

Research report

A new model for dynamic mapping of effective connectivity in task fMRI

Xin Chang [a,b], Zhi-huan Yang [a,b], Wei Yan [a,b], Ze-tao Liu [a,b], Cheng Luo [a,b,c,*], De-zhong Yao [a,b,c,*]

[a] The Clinical Hospital of Chengdu Brain Science Institute, MOE Key Lab for Neuroinformation, School of Life Science and Technology, University of Electronic Science and Technology of China, Chengdu, People's Republic of China
[b] Research Unit of NeuroInformation, Chinese Academy of Medical Sciences, Chengdu 2019RU035, People's Republic of China
[c] High-Field Magnetic Resonance Brain Imaging Key Laboratory of Sichuan Province, University of Electronic Science and Technology of China, Chengdu, People's Republic of China

ARTICLE INFO

Keywords:
Dynamic effective connectivity
Psychophysiological interactions
Sliding window

ABSTRACT

Whole-brain dynamic functional connectivity is a growing area in neuroimaging research, encompassing data-driven methods for investigating how large-scale brain networks dynamically reorganize during resting states. However, this approach has been rarely applied to functional magnetic resonance imaging (fMRI) data acquired during task performance. In this study, we first combined the psychophysiological interactions (PPI) and sliding-window methods to analyze dynamic effective connectivity of fMRI data obtained from subjects performing the N-back task within the Human Connectome Project dataset. We then proposed a hypothetical model called Condition Activated Specific Trajectory (CAST) to represent a series of spatiotemporal synchronous changes in significantly activated connections across time windows, which we refer to as a trajectory. Our finding demonstrate that the CAST model outperforms other models in terms of intra-group consistency of individual spatial pattern of PPI connectivity, overall representational ability of temporal variability and hierarchy for individual task performance and cognitive traits. This dynamic view afforded by the CAST model reflects the intrinsic nature of coherent brain activities.

1. Introduction

Functional magnetic resonance imaging (fMRI) has played a paramount role in cognitive research over the past few decades, shedding light on how individual differences in behavioral attributes are associated with specific brain structures and functions (Zhao et al., 2023). Connectome-based analyses usually focus on resting-state fMRI (van den Heuvel and Hulshoff Pol, 2010). However, there are reasons to suspect that this state may be excessively unconstrained to provide a precise view of cognitive processing (Finn et al., 2017; Gonzalez-Castillo et al., 2021). Acquiring fMRI data while subjects actively perform specific tasks (task state fMRI, tfMRI) can be used to explicitly manipulate their brain state and obtain information about the FC patterns associated with cognition and behavior (Greene et al., 2018). Indeed, apart from PPI, other methods may face challenges in defining task activation for FC or overcoming limitations imposed by hypothesis–driven approaches and model complexity when analyzing large–scale networks (Stephan et al., 2010).

The central role of dynamic neuronal signaling in adaptive cognition and behavior is now widely recognized (Chang and Glover, 2010; Hebb, 1949). Therefore, multiple methods have been proposed to capture the dynamic FC (dFC) in the brain under different task conditions. One such development is the sliding-window approach, which involves computing a metric characterizing FC over gradually shifted time windows of data (Allen et al., 2014). Most statistical analysis for dFC assume that network density and sparsity are fixed, in contrast to the temporal variability of connection strength (Shine et al., 2015). However, emerging methodologies have demonstrated that the connectivity between brain regions is highly dynamic, enabling the emergence and disappearance of transient functional repertoires through time (Hutchison et al., 2013). What is even more unsatisfactory is the fact that most current research paradigms, such as the Chronnectome (Calhoun et al., 2014), which aim to simultaneously consider temporal and spatial changes in time-varying research, still analyze these two aspects independently (Iraji et al., 2019; Liu et al., 2020).

In this study, we proposed a unified framework for a context-

* Correspondence to: No.2006, Xiyuan Ave, West Hi-Tech Zone, Chengdu, Sichuan 611731, People's Republic of China.
E-mail addresses: Chengluo@uestc.edu.cn (C. Luo), dyao@uestc.edu.cn (D.-z. Yao).

https://doi.org/10.1016/j.brainresbull.2024.110938
Received 17 October 2023; Received in revised form 20 March 2024; Accepted 1 April 2024
Available online 17 April 2024

dependent, model-based, data-driven dynamic large-scale effective network analysis. We then represented and validated a hypothetical model as a series of spatiotemporal synchronous changes in connections that are activated by specific task conditions. We refer to these changes as a trajectory and entire model as Condition Activated Specific Trajectory (CAST). Briefly, we combined a generalized form of context-dependent psychophysiological interactions (gPPI) with the sliding-window approach. To represent the hypothetical model, we first explain the hypothesis by assuming that no connection necessarily remains activated and no node necessarily keeps connected throughout the duration of any condition. Then, by introducing the global null hypothesis (H_0), the connection was not activated in any of time window. The alternative hypothesis (H_1) would be the connection was activated at least in one time window, which is properly fit our model. At last, we validated the CAST model by using tfMRI data from the Human Connectome Project (HCP; S1200 release). Our focus was on assessing the superior model performance in terms of intra-group consistency and overall representational ability (ORA) for individual task performance of each condition and cognitive traits. This evaluation was done in contrast to other models used as controls.

2. Methods

2.1. HCP data selection

Our dataset comes from the S1200 release of the HCP (Van Essen et al., 2012). We collected data from 191 participants, including tfMRI data for the working memory task (N-back) of seven major domains (Barch et al., 2013) with corresponding measures of task performance in the form of reaction time (RT) and accuracy (ACC) for each condition. We also obtained cognitive measures for accessible subdomains such as episodic memory, cognitive flexibility, and inhibition (S1 Table). We excluded 45 subjects based on the quality control issues identified by the HCP, namely issue code A (anatomical anomalies), issue code B (segmentation and surface QC), and issue code C (data partially acquired during a period of head coil instability), leaving us with data from 146 individuals.

2.2. HCP n-back working memory task

During the working memory task, participants were presented with blocks of trials involving four types of pictures depicting places, tools, faces, and body parts. We had access to data for two runs through phase encoding in the left-to-right and right-to-left directions, each containing four blocks (one for each image type) lasting 27.5 seconds over a period of 301 seconds (total of 405 frames). Half the blocks used a 2-back task, while the other half used a 0-back task.

2.3. Data preprocessing

We obtained tfMRI data preprocessed using the minimal preprocessing pipelines of HCP (Glasser et al., 2013), which involve gradient unwarping, motion correction, field map based EPI distortion correction, brain-boundary-based registration of EPI to structural T1-weighted scan, non-linear (FNIRT) registration into MNI152 space, and grand-mean intensity normalization. For subsequent volume-based analysis, we applied spatial smoothing with a Gaussian kernel of 4 mm full width at half maximum by using SPM 12 (https://www.fil.ion.ucl.ac.uk/spm/software/spm12/).

Because unrelated behavioral variables can confound the calculation of ORA, we only relied on the cognitive category of behavioral measures and performances (ACC and RT) for each condition. We discarded the measure of delay discounting, because the available items are difficult to directly convert into simple and easily understandable metrics. The Penn Progressive Matrices (PMAT24) for fluid intelligence, only indicated the total number of skipped items. The Variable Short Penn Line Orientation Test (VSPLOT) for spatial orientation, and the Penn Word Memory Test (IWRD) for verbal episodic memory, only provide the percentage of correct responses. Thus, we excluding these items after covert them into ACC, hit and false alarm rates (FAR).

2.4. Condition activated specific trajectory (CAST) analysis

To operationalize CAST model, we established a pipeline involving four Steps (Fig. 1). First, we defined whole-brain seeds/regions of interest (ROIs) and extracted averaged blood oxygenation level dependent (BOLD) signal as physiological term into model. We utilized the well-documented atlas proposed by Jiang and collaborators (Fan et al., 2016), which segments the cerebrum into 246 anatomical regions. For each subject, we extracted the averaged BOLD time series of all voxels within a 6 mm radius of the centroid coordinates in each brain region by using singular value decomposition (SVD) method. Before incorporating these seed time-series signals into the modeling analysis, we also regressed representative signals within white matter and the cerebrospinal fluid using the first eigen-variate of probabilistic templates generated by SPM 12 after Gaussian-weighted high-pass filtering with a cutoff of 200 s (Barch et al., 2013).

The second Step involved construction of the whole-brain PPI model. We adopted the processing functions of gPPI toolbox (https://www.nitrc.org/projects/gppi) on the level of brain regions (Gerchen et al., 2014) for each subject. Briefly, we demeaned the time series containing the timing of stimulus for each condition execution and convolved it with Canonical Hemodynamic Response Function (HRF) to form the psychological terms (psycho) in the model. For each seed, the interaction terms (PPI) are constructed by multiplying the averaged signal with time series of each task condition after deconvolved it with the HRF. Then, the interaction terms are also need to go through demean and convolve with the HRF again. At last, the psycho, physiological and PPI terms targeting to each of regions were incorporated into one multiple linear regression (MLR) model.

The third Step involved process for dynamic whole-brain PPI analyses. Firstly, the MLR model was adjusted to account for collinearity among regressors and serial autocorrelations by introducing the pre-whiten procedure implemented in SPM. Beta values of each PPI for different condition (β_4 and β_5 in this study, Fig. 1 Step 2) were estimated using MLR and saved in a full connectivity matrix between all seeds. Dynamic analysis was conducted with the segmented model by using sliding window approach. We used a rectangular window (width of 35 frames) that only covered one block size in the task. Combined with the minimum moving size (step of 1 frame) for capturing the finer movement trajectories of spatiotemporal synchronous changes in connections, resulted in $W = 371$ windows ((total – width) / step + 1). We excluded entire segmented model for which any of time series of each condition is a constant vector in case the issues such as model instability and multicollinearity.

In the fourth Step, we introduced the global null hypothesis (H_0) for each of elements across the PPI matrices of time windows, excluding the diagonal, to test if a connection was not activated throughout a performed condition. Then the alternative hypothesis (H_1) can be represented the characteristic of spatiotemporal synchronous for all connections activated by one task condition. In this way, we start by reshaping all matrices of time windows with one condition, which containing statistical t-values that are calculated by dividing the effect sizes (β_4 or β_5) by the standard error, into a single matrix. Its rows represent the time windows and columns represent the connections. To represent a connection across time windows and avoid the influence of positive and negative signs on each other, we selected the minimum negative and maximum positive t-values from the activated connections, as these values can reject the H_0. Then we proceeded to perform False Discovery Rate (FDR) multiple comparison correction separately for these extreme t-values with different signs. The correction was applied with a significance level of $p \leq 0.05$. The resulting thresholds were then

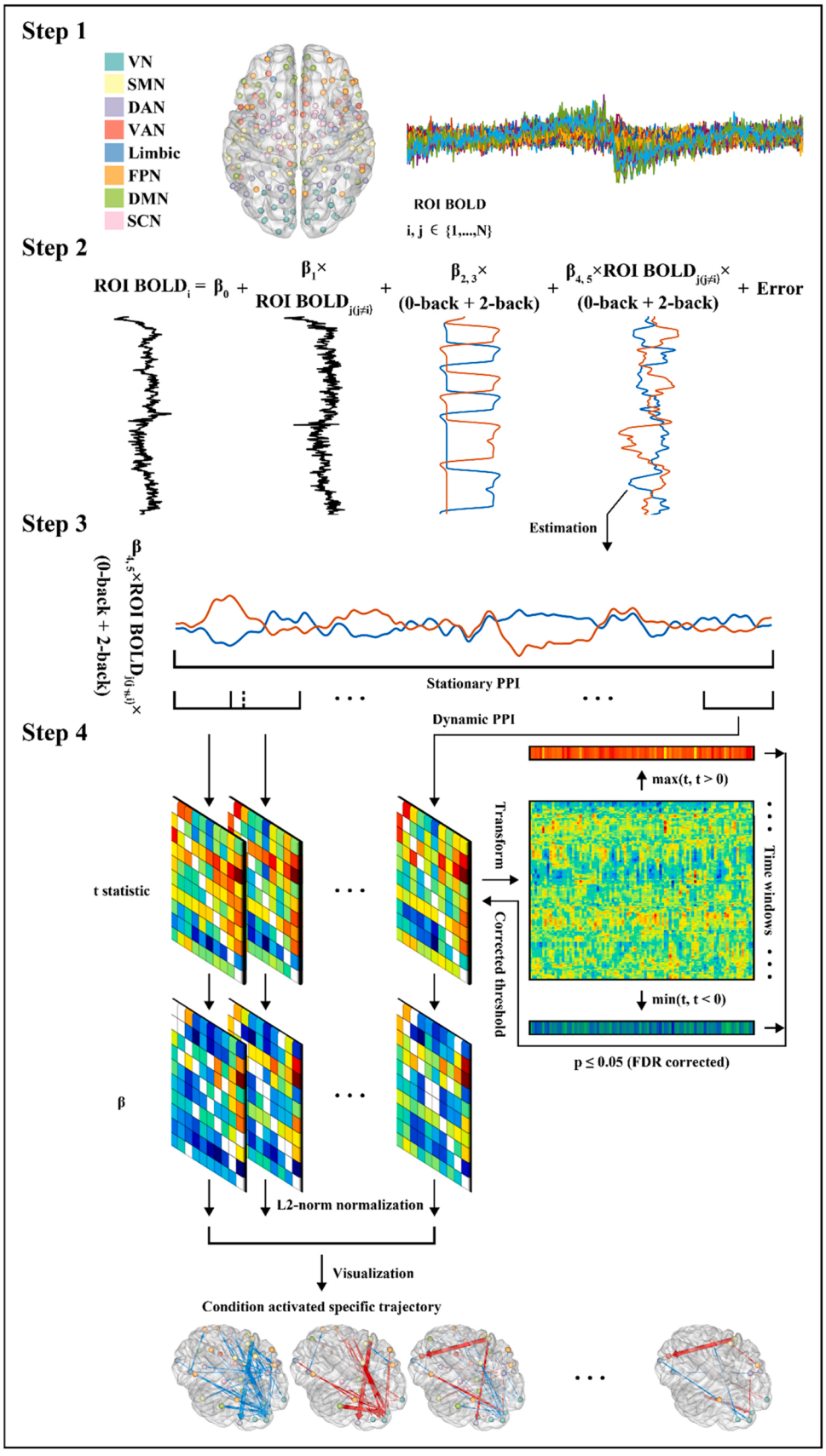

(caption on next page)

Fig. 1. Fundamental steps of the pipeline for CAST analysis. Briefly the pipeline involves the following Steps: Step 1: extracting the averaged BOLD signals using a customized whole-brain parcellation; Step 2: Constructing the MLR model, which includes the separate time series for each condition (psycho), the averaged BOLD signs of a region (physiological), interaction terms for each condition, and covariates; Step 3: estimating the whole-brain PPI for each segment model using a sliding window approach; Step 4: filtering out spurious connections and constructing the CAST model to represent the hypothesis of spatiotemporal synchronous changes by using the adopted global analysis. VN, visual network; SMN, somatomotor network; DAN, dorsal attention network; VAN, ventral attention network; FPN, frontoparietal network; DMN, default mode network; SCN, sub-cortical network.

applied in the process of sparsification for each time windows. Connections that fell below the thresholds were considered spurious (non-significant) and were replaced with zero. From introducing the global null hypothesis up to replacing spurious connections with zeros, we referred to these processes as "adopted global analysis". We enhanced the continuity between time windows by standardizing the retained connections (β_4 or β_5) within each time window using the L2–norm. This method does not impose consistent network density across different time windows. The remain time windows, along with the activated connections that surpass the corrected thresholds, form the CAST network.

2.5. Estimating dynamic characteristics of CAST

Within each matrix of time window, brain regions are connected in three-dimensional (3D) space. CAST captures a series of spatiotemporal synchronous changes in significantly activated connections across time windows, i.e., in a four-dimensional (4D, 3D + time dimension) manner. For each subject, the temporal variability (TV) was analyzed by calculating the standard deviations for each (i) connection (e) across the time windows (w) that were activated (non-zero, ∃) as follow:

$$\mathrm{TV}_i = \sigma\left(\exists\left(e_{i,w}\right)\right)\# \tag{1}$$

The spurious connections were all replaced with zeros. Then, the overlap rate (OR), which serves as an indicator of the spatial variability in connectivity, can be calculated directly as the ratio of the number of activation (w) for each (i) connection to the total number of time windows (W), as follow:

$$\mathrm{OR}_i = \frac{\sum \exists(w_i)}{W}\# \tag{2}$$

Finally, by evaluating whether elements in the OR matrix are zero, we obtained a binarized individual 3D spatial pattern matrix, which was used for subsequent analysis of intra-group consistency.

2.6. Characterizing the dynamical hierarchy

According to the hypothesis of CAST, in which no connection necessarily remains activated and no node necessarily keeps connected throughout the duration of any condition, the sizes of connected nodes and network density may vary across time windows as a result. Due to the effective connectivity matrix, we calculated the outdegree and indegree of each node within every time window. Then, we defined a dynamical topological characteristic (D) that describes the different types of nodes (n) in each directed asymmetric matrix of the time windows (w) as follow:

$$D_{n,w} = \frac{outdegree_{n,w} - indegree_{n,w}}{outdegree_{n,w} + indegree_{n,w}}\# \tag{3}$$

Notably, if a node only has outdegree without indegree, then this node is referred to as the starting point with $D = 1$; Conversely, if a node only has indegree without outdegree, then this node is referred to as the ending point and $D = -1$. When $D = 0$, the node is referred to as a full intermediate point. In other cases, when D is a non-integer within the range of −1–1, the node is also referred to as an intermediate point, indicating its representation and drive capability for the starting/ending point or outflow/inflow circuits.

In this way, we further construct the dynamical hierarchy based on nodes with different values of D. To gain more insights into this hierarchical structure, we distinguished different methods based on two considerations: 1) whether to only accept the full intermediate point by replacing non-integer D values with 0; 2) calculating the value of D in each time window and averaging it, or directly computing it within the individual 3D spatial pattern (Table 1).

To compare these methods and facilitate the matching with subsequent analysis, we extracted ten global metrics. These metrics were employed to provide a more generalized depiction of the dynamical hierarchy constructed by the three methods (taTRs, iDTCs, and taDTCs) separately.

1) Mobility: this metric describes the capacity or tendency for information to flow from any direction in the dynamical hierarchical spatial layout. It quantifies the extent to which the mean absolute value of D, obtained from all existing nodes (N), approaches 1.

$$\mathrm{Mobility} = \frac{\sum_i |D_i|}{N}\# \tag{4}$$

2) Tropism: this metric indicates the representation strength for a fully out/inflow network within the dynamical hierarchy. It is determined by the average value approaching either 1 or −1.

$$\mathrm{Tropism} = \frac{\sum_i D_i}{N}\# \tag{5}$$

3) Dispersity: this metric describes which set of nodes with outflow ($D > 0$) or inflow ($D < 0$) direction presents a numerical advantage.

$$\mathrm{Dispersity} = \frac{N(D>0) - N(D>0)}{N}\# \tag{6}$$

4) Breadth: this metric reflects the ratio of unique (!) levels within the hierarchy.

$$\mathrm{Breadth} = \frac{N(!(D))}{N}\# \tag{7}$$

5) Span: this metric estimates the dispersion (σ) of unique hierarchy, that is the average deviation from the central level.

Table 1
The methods for constructing the dynamical hierarchy.

		1) Whether to set the non-integer output to 0?	
		Yes	No
2) Initial dimension	3D	Excluded	iDTCs
	4D	taTRs	taDTCs

Note: We did not adopt the method of replacing non-integer values with 0 when analyzing the 3D spatial pattern directly. As the hierarchy only consists of three levels in this situation, we consider this method cannot provide more information about the dynamical characteristic. Therefore, we retained three methods: 1) time averaged topological roles (taTRs); 2) integrated dynamical topological characteristics (iDTCs); 3) time averaged dynamical topological characteristics (taDTCs).

$$\text{Span} = \sigma(!(D))\#$$ (8)

6) Depth: this metric indicates the magnitude of hierarchy by using the difference in extreme values, and rescaling the magnitude range of −1–1.

$$\text{Depth} = \frac{\max(D) - \min(D)}{2}\#$$ (9)

7) Minimal resolution: this metric reflects the smallest spacing in the dynamical hierarchy with the minimum value of inter-layer (sorted with D from −1–1) differences described by the first order difference (Δ).

$$\text{Minimalresolution} = \min(\Delta(!(D)))\#$$ (10)

8) Mean resolution: this metric describes the average spacing in the hierarchy with the mean of inter-layer differences.

$$\text{Meanresolution} = \mu(\Delta(!(D)))\#$$ (11)

9) Median resolution: this metric describes the median (Me) spacing in the hierarchy.

$$\text{Medianresolution} = \text{Me}(\Delta(!(D)))\#$$ (12)

10) Resolution error: this metric describes the dispersion degree of entire spacing in the hierarchy with the standard error of inter-layer differences.

$$\text{Resolutionerror} = \sigma(\Delta(!(D)))\#$$ (13)

2.7. Different models to compare with the CAST model

To validate the hypothesis of the CAST model, we established three control models for comparison, in which the Step 3 and 4 in the CAST pipeline were adjusted:

1) Stationary model, which included Steps 1–2 and estimated β_4 and β_5 matrices directly using the complete time series.
2) Dynamic gPPI model 1, which included all steps, differed from the CAST model in the application of corrected thresholds during the sparsification process for each time window. In this model, a connection with corresponding sign (+/–) across time windows was considered activated if the global null hypothesis H_0 was rejected.
3) Dynamic gPPI model 2, based on the CAST model, employed a criterion where if the number of activations for a connection with its corresponding sign (+/–) across time windows was less than 50% of the total windows, the connections with their corresponding sign would be all replaced with 0. This percentage (50%) was considered to possess the highest generalization ability as it required at least two time windows in dynamic research.

We excluded zero values from the calculation of TV in the Dynamic gPPI model 1 and 2, as well as the CAST model, in which the effect of OR can be investigated independently. To validate this independence, we established an additional control model named CAST model 2, which included zero values in the calculation.

2.8. Evidences for validating the CAST model

We relied on three primary evidences to validate CAST compared to other four models (Fig. 2). Notably, the assessment for the independence of individual TV and OR for each model is not as primary evidence and is validated in the supplemental material instead. For Evidence 1, we calculated the intra-group consistency of individual spatial pattern by determining the median percentage of overlap among all connections within different models. To estimate the significance of superior consistency, we conducted a permutation test (S1a Fig) with 2000 iterations. Briefly, we randomly select one model for each subject with replacement in each iteration. The consistency is then calculated for each random sample to construct a null distribution. The significance of each model was determined by the number of its consistency values smaller than the random sample, divided by the number of iterations

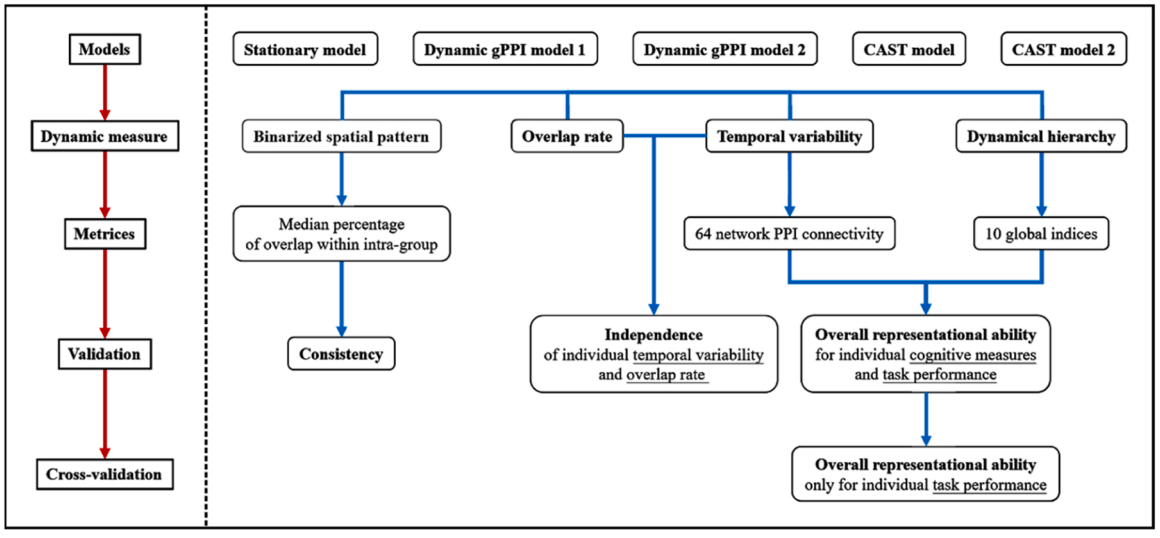

Fig. 2. Flowchart of the validation process for the CAST model. After preprocessing the tfMRI data, the stationary model and the CAST model were initially calculated using either the complete time series or fixed window length. Afterwards, the corrected thresholds were used to construct additional models, including Dynamic gPPI model 1 and 2, as well as CAST model 2. The next step involved measuring the binarized spatial pattern, matrixes of overlap rate and temporal variability, and hierarchy for nodes. The median percentage of overlap within the intra-group was computed as a measure of consistency for Evidence 1. Simultaneously, the correlation between the individual overlap rate and temporal variability was determined. The overall representational ability of temporal variability and hierarchy for individual cognitive measures and task performance were analyzed as the Evidence 2 and 3. Finally, a cross-validation process was conducted exclusively for evaluating the overall representational ability in relation to individual task performance.

(2000).

For Evidence 2, we compared the ORA of each model in temporal variability of network PPI connectivity. Briefly, we first extracted the average TV of PPI connectivity within intra-networks and inter-networks by using Yeo's parcellation of networks (Yeo et al., 2014). Then, we calculated the Pearson's correlation between the TV and 28 behavioral data (individual cognitive traits and task performance) and saved the significant correlation coefficients in a matrix for each model. The rows of correlation matrix represent the averaged TV within intra-network and inter-network, while the columns represent the different behavioral data. To estimate the significance of superior ORA, we performed a permutation test (S1b Fig) with 2000 iterations. In each iteration, we randomly exchanged the rows of matrix of models. The ORA of each model is calculated for each random sample using four indexes to construct null distribution. These indexes including: 1) the average absolute value of significant correlation coefficients (β), 2) the average absolute value of significant statistical t-value (t) derived from β, 3) the sum of eigenvalues of each matrix and 4) the number of significant correlations. The significance of each ORA index was determined by the number of its values smaller than the random sample, divided by the number of iterations (2000).

For Evidence 3, we compared the ORA of each model using ten global metrics extracted from the dynamical hierarchy. The correlation matrix was calculated with these global metrics, not TV. The rest of process was the same as in Evidence 2.

3. Results

3.1. Evidence 1: Intra-group consistency of spatial pattern

The intra-group spatial pattern consistency for all models, along with their significance, is summarized in Table 2. We found that regardless of task condition (0-back or 2-back), the Dynamic gPPI model 1, CAST model and 2, which shared the same spatial pattern, exhibited significantly ($p \leq 0.001$) superior consistency reaching almost 100%. In contrast, the consistency of Stationary model and Dynamic gPPI model 2 was barely close to 10%.

S2 and S3 Figs provided additional details about the characteristics of the spatial pattern for the Stationary model, Dynamic gPPI model 2 and CAST model. Briefly, only the percentage of overlap within the CAST model surpassed the threshold ($p \leq 0.05$, FDR corrected). Apart from the significance, the Stationary model shared a similar spatial pattern. Therefore, it is reasonable to believe static effect represents the magnitude of the average dynamic effect and highest overlap rate. Lastly, we examined the significance of the network PPI spatial of CAST model using the permutation test (S1c Fig).

Table 2
The performance of each model with the Evidence 1.

Condition	Model	Consistency
0-back	Stationary model	0.06849
	Dynamic gPPI model 1	0.9863***
	Dynamic gPPI model 2	0.00685
	CAST model	0.9863***
	CAST model 2	0.9863***
2-back	Stationary model	0.06849
	Dynamic gPPI model 1	0.9863***
	Dynamic gPPI model 2	0.0137
	CAST model	0.9863***
	CAST model 2	0.9863***

Note: asterisks (*) indicate significance level from the permutation test: * for $p \leq 0.05$, ** for $p \leq 0.01$, *** for $p \leq 0.001$.

3.2. Evidence 2: The overall representational ability of temporal variability in network PPI connectivity

As seen in Table 3, only two CAST models exhibited statistically significant results for all indices of the ORA by using permutation test. Although the Dynamic gPPI model 1 shared the same spatial pattern with CAST models, only the sum of eigenvalues and the number of significant correlations achieved mild significance. While the indexes produced by the CAST model were overall lower than model 2, the CAST model outperformed model 2 when only including the task performance as the behavioral data (S2 Table).

We also observed that only these three models, Dynamic gPPI model 1, CAST model and 2 with the same spatial pattern were able to surpass the threshold ($p \leq 0.05$, FDR corrected) in both one-sample t tests and permutation tests (S1a Fig) for TV matrices. However, they did not share significant spatial pattern (S4 and S5 Figs). The main differences were primarily observed in the somatomotor network (SMN), ventral attention network (VAN) and frontoparietal network (FPN) as inflow (modulated) networks. It is suspected that the Dynamic gPPI model reserved most of spurious connections, as FPN appeared to play an insignificant role in this cognitive task.

We further validate the optimal ORV of CAST model 2 in TV by investigating the independence of TV and OR for each model. For each subject, we first performed a Pearson's correlation analysis between TV and OR matrix, excluding the diagonal and positions with a value of 0. Then, we conducted a one-way rANOVA and post hoc tests for these coefficients of each model. The results (S6 Fig, S3 and S4 Tables) revealed significant main effect ($p \leq 0.001$) and differences among the models ($p \leq 0.001$) except for the comparison between Dynamic gPPI model 1 and 2, regardless of the conditions (0-back and 2-back). In contrast to CAST model 2, which exhibited the hightest correlation, CAST model effectively distinguished between the effects of TV and OR. The mean correlation values of CAST model, Dynamic gPPI model 1 and 2 were all closed to 0. However, in contrast to Dynamic gPPI model 1 exhibited the most compressed distribution, while Dynamic gPPI model 2 had the widest distribution (S6 Fig).

3.3. Evidence 3: The overall representational ability of the dynamical hierarchy

We devised three methods to capture the overall dynamical topological characteristics for each node and subsequently constructed different hierarchical structures (Fig. 3). In terms of the distribution range of characteristic extracted from each method, we observed that the spatial layout provided by the iDTCs method was relatively flat, with only a few nodes showing prominent D. The dynamical hierarchy constructed by the taTRs method indicated that almost all observed nodes were in the outflow direction. Therefore, it is more rational to acknowledge that the taDTCs method captured more comprehensive hierarchical information. Notably, these two time-averaged (ta) methods refer to the spatiotemporal synchronous changes in connected nodes. By applying the same procedure to validate the ORA with TV, using different combinations of ten global indices extracted from each hierarchy and PPI models, we observed that only the combination of CAST model and the taDTCs method showed full significance in four indexes of ORA (Table 4). This significant superiority was also cross-validated when including only the task performance as the behavioral data (S5 Table).

4. Discussion

In this study, we proposed a new model called the Condition Activated Specific Trajectory (CAST) model to capture the spatiotemporal synchronous changes in connections that activated by specific task conditions. The abbreviation CAST highlights the assumption of a transmission property, in which no connection necessarily remains

Table 3
The performance of each model with the Evidence 2.

Condition	Model	β	t statistic	Eigenvalue	Number
0-back	Stationary model	0	0	0	0
	Dynamic gPPI model 1	0.01857	0.22749	22.578*	167*
	Dynamic gPPI model 2	0.00811	0.08921	13.666	66
	CAST model	0.02084**	0.25518**	22.952**	188**
	CAST model 2	0.02561***	0.31463***	24.450***	218***
2-back	Stationary model	0	0	0	0
	Dynamic gPPI model 1	0.01830	0.22435	22.025*	162
	Dynamic gPPI model 2	0.00973	0.10459	16.056	80
	CAST model	0.02283**	0.27963**	24.002***	205**
	CAST model 2	0.02530***	0.31081***	23.410**	214***

Note: asterisks (*) indicate significance level from the permutation test: * for p≤0.05, ** for p≤0.01, *** for p≤0.001.

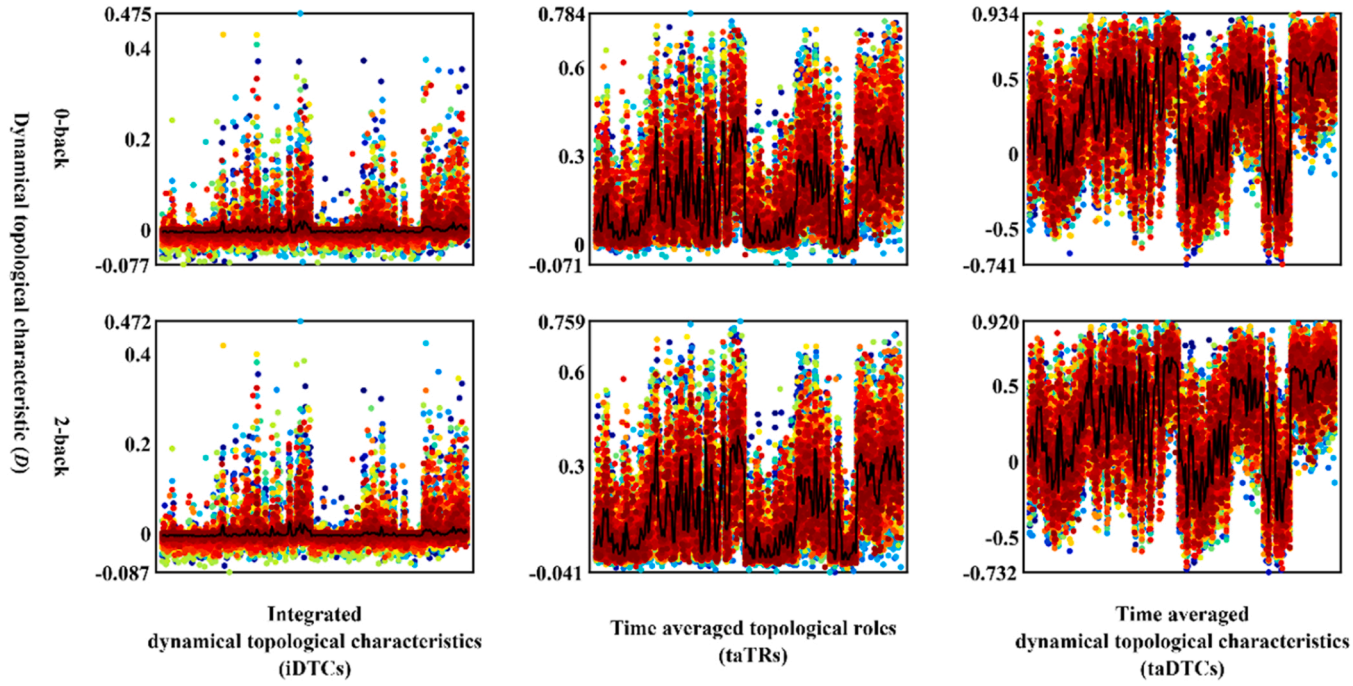

Fig. 3. Dynamical hierarchy of CAST model using three different methods. Different subgraphs correspond to different combinations of task conditions (0-back or 2-back) and the method used to capture the overall dynamical topological characteristics (*D*) for each node (column). Each color of nodes represents one subject, and the black line indicates the group–averaged *D*.

activated and no node necessarily keeps connected throughout the duration of any condition, and circuits can be connected in a four-dimensional manner. To validate this assumption of the CAST model, we constructed four additional models and compared them with multiple lines of evidences from three different aspects: intra-group consistency of spatial pattern of connectivity, overall representational ability (possessed meaning) with temporal variability of network PPI connectivity and dynamical hierarchy.

As the fundamental algorithm used to analyze task-dependent connectivity in this study, PPI can be regarded as a condition specific change in effective connectivity, under a simple general linear model interregional coupling (Di et al., 2021). The functional connectivity, in which the correlation between time courses of different regions are directly analyzed, is highly contributed by the spontaneous neural activity (Biswal et al., 1995), or other common factors such as common anatomical connectivity (Honey et al., 2009), common neurovascular responses (Sivakolundu et al., 2020), physiological noises (Weissenbacher et al., 2009), or head motion (Power et al., 2012). Therefore, effective connectivity analysis provides more informative and valuable insight into whether connections are modulated by task conditions. In addition to the PPI method, other model approaches such as dynamical causal modeling (DCM) (Friston et al., 2003) and Granger causality analysis (GCA) can also estimate the underlying causal structure. However, these methods have certain limitations (Gerchen et al., 2014). For instance, DCM is computationally expensive, and is restricted to specific models with only a few nodes. GCA estimates the causality by taking time lags into account, making it is difficult to separate different condition context and critical for incorporating the signal itself (Smith et al., 2011). Besides, PPI has bridged the gap between activation and connectivity analysis and has matured in analysis for the task-dependent connectivity changes in a whole-brain manner (Cocchi et al., 2013).

To be compatible with the dynamic analysis of PPI, we decided on using sliding-window. Other available methods, such as multiplication of temporal derivatives (MTD) (Shine et al., 2015), and co-activation (CAP) (Liu et al., 2013) undermine the advantages of PPI. Previous research with PPI-CAPs demonstrated high consistency in effective connectivity patterns across subjects and time, and explicitly revealed transients in tracking connectivity patterns (Freitas et al., 2020), which should benefit naturalistic paradigms. However, the overlaid averaged PPI map without estimation in MLR is unable to provide any information related to flow direction. Considering the concerns raised by the selection of sliding-window parameters, multiple studies have indicated a

Table 4
The performance of each model with the Evidence 3.

Condition	Model	Dynamical hierarchy	β	t statistic	Eigenvalue	Number
0-back	Stationary model	iDTCs	0.00643	0.07836	1.899	10
		taTRs	0.00123	0.01493	0.559	2
		taDTCs	0.00643	0.07836	1.899	10
	Dynamic gPPI model 1	iDTCs	0.02679	0.32612	5.759	41
		taTRs	0.00128	0.01560	0.585	2
		taDTCs	0.02649	0.32339	5.451	39
	Dynamic gPPI model 2	iDTCs	0.02790	0.33995	4.491	42
		taTRs	0.02913	0.35508	4.747	43
		taDTCs	0.02919	0.35627	4.823	42
	CAST model	iDTCs	0.02679	0.32612	5.759	41
		taTRs	0.03052	0.37329	5.271	42
		taDTCs	0.04419**	0.54232**	7.675**	58*
	CAST model 2	iDTCs	0.02679	0.32612	5.759	41
		taTRs	0.03052	0.37329	5.271	42
		taDTCs	0.04419**	0.54232**	7.675**	58*
2-back	Stationary model	iDTCs	0.00124	0.01513	0.801	2
		taTRs	0	0	0	0
		taDTCs	0.00124	0.01513	0.801	2
	Dynamic gPPI model 1	iDTCs	0.03084	0.37689	6.545	45
		taTRs	0.00128	0.01560	0.585	2
		taDTCs	0.03086	0.37676	5.308	45
	Dynamic gPPI model 2	iDTCs	0.01490	0.18110	4.731	23
		taTRs	0.02828	0.34415	5.839	43
		taDTCs	0.02238	0.27249	5.592	34
	CAST model	iDTCs	0.03084	0.37689	6.545	45
		taTRs	0.02545	0.31165	6.586	35
		taDTCs	0.04812**	0.59261**	8.348**	60**
	CAST model 2	iDTCs	0.03084	0.37689	6.545	45
		taTRs	0.02545	0.31165	6.586	35
		taDTCs	0.04812**	0.59261**	8.348**	60**

Note: asterisks (*) indicate significance level from the permutation test: * for $p \leq 0.05$, ** for $p \leq 0.01$.

limited extent of problems (Choe et al., 2017; Cohen, 2018). Therefore, in this study we proceeded without hesitation to establish the sequence of model construction and segmentation. We excluded models with convolved psychological regressors that resulted in constant series after segmentation. From an algorithmic point of view, in addition to using a rectangular window with a length that merely covered the duration of each task block (35 frames), we employed a step size of 1 frame to capture finer changes.

Currently, most statistical analysis for dFC assume that network density remains stable (Shine et al., 2015). On the contrary, a study using spatial ICA over a short sliding window found that the default mode network (DMN) changes significantly over time, and reported a considerable degree of spatial heterogeneity, suggesting that no voxel was continuously connected to the primary DMN activity (Kiviniemi et al., 2011). Although the Chronnectome was introduced as a model for observing nodal activity and changes in connectivity patterns over time (Calhoun et al., 2014), there is still dissatisfaction with the approaches in this field. Typically, temporal variability is detected with fixed or full connections among nodes, while spatial variability is assessed through the dynamic switching of module partition (modular variability) for specific nodes, analyzed within each window at the start by setting a network density (Liu et al., 2020). Thus, our hypothetical CAST model is assuming that no connection necessarily remains activated and no node necessarily keeps connected throughout the duration of any condition by introducing a global null hypothesis to test as following.

Dynamic gPPI model 1 and CAST model exhibit significantly greater intra-group consistency compared to typical Stationary model and Dynamic gPPI model 2. This superiority is laid on the group-level statistical analysis, where a higher median consistency indicates a larger accounted sample. The reason for conducting group-level analysis on the sparsified individual connectivity matrix is that this approach can effectively avoid the inclusion of spurious connections, thereby increasing the reliability and interpretability of the results. An extreme counterexample is when the individual connectivity beta values are not significant but have very low intra-group connection standard errors, resulting in a meaningless group-level significance still. That is also why in recent years, an increasing number of studies have appealed to effect sizes rather than excessive reliance on statistical values (Wasserstein and Lazar, 2016).

Another counterexample is when the individual connectivity beta values are predominantly significant, yet they exhibit diverse signs cross time windows, ultimately resulting in group-level insignificance. Considering the generalization ability of model, we denied the model using one-sample t tests, due to restriction of the sample size. Additionally, during the initial pretest, we observed that no single connection remained significant under the conjunction analysis for individual time windows. This led us to employ the Dynamic gPPI model 2 to capture the overall significance, while controlling for the criterion of the number of significant time windows for each connection. We selected 50% as the criterion with hightest generalization ability in dynamic analysis, as it requires a minimum of two samples. Importantly, both Dynamic gPPI model 1 and 2 were designed to test the hypothesis, but they differed in the level of strictness for controlling overall significance in two directions.

When comparing the overall representational ability of temporal variability in network PPI connectivity, although the Dynamic gPPI model share the same 3D spatial pattern with CAST model, it fails to outperform. This result further confirms the presence of spurious connections and their confounding effect on interpretation. Additionally, through the validation of the independence of TV and OR, we not only observed the highest correlation in CAST model 2, but also confirmed the superior interpretability due to the inclusion of spatial variability of connections represented by OR. Taken together, these findings validate the hypothesis of trajectory.

Regarding the TV matrix of the CAST model, clear differences between the two task conditions were restricted to the FPN network, in line with the activation count maps for 2-back versus 0-back (Barch et al., 2013). Moreover, in a previous study of the dynamic causal brain pathway associated with working memory, the FPN was found to distinguish between working memory load and predict performance,

suggesting that causal outflow and inflow hubs are all maintained in the FPN (Cai et al., 2021). Although we are not the first to report that working memory tasks carry more predictive power for such cognitive abilities (Jiang et al., 2020), our results represent the first attempt at interpreting their meaning and potential, because the trend of variability observed with PPI differs from that reported by dFC studies, which consistently observed a general decrease when an individual is in a constrained cognitive environment (Chen et al., 2015; Cohen, 2018).

Inspired by a recent study that identified the modular architectures of dynamic functional networks (Liu et al., 2020), we attempted to validate the CAST by comparing the ORA of hierarchy that constructed based on the symmetric variation rate between out-degree and in-degree for each node. We referred to this rate as the dynamical topological characteristic, as it indicates the dynamical feature of a node during information flow. Specifically, it considers the basic types of nodes in a directed graph: staring point, intermediate point and ending point. By comparing the time-averaged (ta) method with the integrated method, which directly analyzes the characteristics in 3D spatial pattern rather than analyzing them in each window and averaging the results, we validate the spatiotemporal synchronous change in connected nodes.

Our study has several limitations. First, we relied solely on one dataset (HCP), and data from only one task. The purpose of this pilot study was to propose and validate a new model in a basic manner. Therefore, we deliberately chose to use this well-documented task from an open dataset. In future research, we will expand our validation by incorporating additional tasks and datasets. Secondly, the impact of parameters within the framework, such as window length, threshold with sparsity, and HRF, as well as the inclusion of other connectivity indices beyond temporal variability, and mutual corroboration with other hierarchical structures related to our novel dynamical hierarchy, were not thoroughly examined. We intend to address these limitations in future research. Thirdly, it would be beneficial to compare our methods with other approaches such as independent vector analysis, dFC, or multilayer networks. Fourthly, as the emerging activation and network studies in the brain white matter (Ji et al., 2023, 2017; Jiang et al., 2022), it is crucial to investigate the influence of CAST, especially on the overlap rate and hierarchy of these spatial arrangements.

5. Conclusion

We presented a novel framework that can analyze the context-dependent, model-based, data-driven, dynamic large-scale modulations of effective connectivity during task performance. By introducing global null hypothesis for each PPI connection cross time-windows, conducting multi-comparison correction for testing the global null hypothesis, and employing the corrected thresholds to exclude the spurious connections in each time-window, we formalized these three processes as adopted global analysis and represented a hypothetical model as a series of spatiotemporal synchronous changes in connections that activated by specific task conditions. This model, referred to as Condition Activated Specific Trajectory (CAST), is validated through comparisons with intra-group consistency of individual spatial patterns of PPI connectivity, overall representational ability of temporal variability and hierarchy, among four models that constructed by controlled the process of sparsification and calculation for temporal variability. Finally, the dynamic view afforded by the CAST model reflects the intrinsic nature of coherent brain activities.

Ethical approval

The Review Board and Ethics Committee of the University of Electronic Science and Technology of China approved this study to request access to data collected by the WU-Minn HCP (Washington University – University of Minnesota Consortium of the Human Connectome Project) and agree to the Open Access Data Use Terms.

Funding

This work was funded by a grant from the National Nature Science Foundation of China (61933003, U2033217, 62201133 and 62003058), China Postdoctoral Science Foundation (2021TQ0061), and the CAMS Innovation Fund for Medical Sciences (CIFMS) (No. 2019-I2M-5–039), Project of Science and Technology Department of Sichuan Province (2022NSFSC1320, 23NSFSC0016), the Fundamental Research Funds for the Central Universities (ZYGX2022YGRH017).

CRediT authorship contribution statement

Xin Chang: Writing – original draft, Visualization, Validation, Methodology, Investigation, Formal analysis, Conceptualization. **Zhihuan Yang:** Methodology, Investigation, Formal analysis. **Wei Yan:** Methodology, Investigation, Formal analysis. **Ze-tao Liu:** Investigation, Formal analysis. **Cheng Luo:** Writing – review & editing, Supervision, Resources, Project administration. **Dezhong Yao:** Resources, Project administration, Supervision, Writing – review & editing.

Declaration of Competing Interest

The authors declare that there were no conflicts of interest with respect to the authorship or the publication of this article.

Data availability

The data that has been used is confidential.

Acknowledgments

We thank the Human Connectome Project (https://www.humanconnectome.org/) for making the data publicly available.

Code availability

Functional MRI data preprocessing and statistical analyses were performed on the SPM 12, FSL 6 (https://fsl.fmrib.ox.ac.uk/fsl/). Matlab scripts written to perform CAST analysis are available from the authors upon request.

Reporting

This study involved an analysis of existing data rather than new data collection.

Appendix A. Supporting information

Supplementary data associated with this article can be found in the online version at doi:10.1016/j.brainresbull.2024.110938.

References

Allen, E.A., Damaraju, E., Plis, S.M., Erhardt, E.B., Eichele, T., Calhoun, V.D., 2014. Tracking whole-brain connectivity dynamics in the resting state. Cereb. Cortex *24* (3), 663–676. https://doi.org/10.1093/cercor/bhs352.

Barch, D.M., Burgess, G.C., Harms, M.P., Petersen, S.E., Schlaggar, B.L., Corbetta, M., Glasser, M.F., Curtiss, S., Dixit, S., Feldt, C., Nolan, D., Bryant, E., Hartley, T., Footer, O., Bjork, J.M., Poldrack, R., Smith, S., Johansen-Berg, H., Snyder, A.Z., Consortium, W.U.-M.H., 2013. Function in the human connectome: task-fMRI and individual differences in behavior. Neuroimage *80*, 169–189. https://doi.org/10.1016/j.neuroimage.2013.05.033.

Biswal, B., Yetkin, F.Z., Haughton, V.M., Hyde, J.S., 1995. Functional connectivity in the motor cortex of resting human brain using echo-planar MRI. Magn. Reson. Med. *34* (4), 537–541. https://doi.org/10.1002/mrm.1910340409.

Cai, W.D., Ryali, S., Pasumarthy, R., Talasila, V., Menon, V., 2021. Dynamic causal brain circuits during working memory and their functional controllability. https://doi.org/ARTN 3314 Nat. Commun. *12* (1). https://doi.org/10.1038/s41467-021-23509-x.

Calhoun, V.D., Miller, R., Pearlson, G., Adali, T., 2014. The Chronnectome: Time-Varying Connectivity Networks as the Next Frontier in fMRI Data Discovery. Neuron *84* (2), 262–274. https://doi.org/10.1016/j.neuron.2014.10.015.

Chang, C., Glover, G.H., 2010. Time-frequency dynamics of resting-state brain connectivity measured with fMRI. Neuroimage *50* (1), 81–98. https://doi.org/10.1016/j.neuroimage.2009.12.011.

Chen, J.E., Chang, C., Greicius, M.D., Glover, G.H., 2015. Introducing co-activation pattern metrics to quantify spontaneous brain network dynamics. Neuroimage *111*, 476–488. https://doi.org/10.1016/j.neuroimage.2015.01.057.

Choe, A.S., Nebel, M.B., Barber, A.D., Cohen, J.R., Xu, Y., Pekar, J.J., Caffo, B., Lindquist, M.A., 2017. Comparing test-retest reliability of dynamic functional connectivity methods. Neuroimage *158*, 155–175. https://doi.org/10.1016/j.neuroimage.2017.07.005.

Cocchi, L., Zalesky, A., Fornito, A., Mattingley, J.B., 2013. Dynamic cooperation and competition between brain systems during cognitive control. Trends Cogn. Sci. *17* (10), 493–501. https://doi.org/10.1016/j.tics.2013.08.006.

Cohen, J.R., 2018. The behavioral and cognitive relevance of time-varying, dynamic changes in functional connectivity. Neuroimage *180* (Pt B), 515–525. https://doi.org/10.1016/j.neuroimage.2017.09.036.

van den Heuvel, M.P., Hulshoff Pol, H.E., 2010. Exploring the brain network: a review on resting-state fMRI functional connectivity. Eur. Neuropsychopharmacol. *20* (8), 519–534. https://doi.org/10.1016/j.euroneuro.2010.03.008.

Di, X., Zhang, Z.G., Biswal, B.B., 2021. Understanding psychophysiological interaction and its relations to beta series correlation. Brain Imaging Behav. *15* (2), 958–973. https://doi.org/10.1007/s11682-020-00304-8.

Fan, L., Li, H., Zhuo, J., Zhang, Y., Wang, J., Chen, L., Yang, Z., Chu, C., Xie, S., Laird, A. R., Fox, P.T., Eickhoff, S.B., Yu, C., Jiang, T., 2016. The Human Brainnetome Atlas: a new brain atlas based on connectional architecture. Cereb. Cortex *26* (8), 3508–3526. https://doi.org/10.1093/cercor/bhw157.

Finn, E.S., Scheinost, D., Finn, D.M., Shen, X.L., Papademetris, X., Constable, R.T., 2017. Can brain state be manipulated to emphasize individual differences in functional connectivity? Neuroimage *160*, 140–151. https://doi.org/10.1016/j.neuroimage.2017.03.064.

Freitas, L.G.A., Bolton, T.A.W., Krikler, B.E., Jochaut, D., Giraud, A.L., Huppi, P.S., Van De Ville, D., 2020. Time-resolved effective connectivity in task fMRI: Psychophysiological interactions of Co-Activation patterns. Neuroimage *212*, 116635. https://doi.org/10.1016/j.neuroimage.2020.116635.

Friston, K.J., Harrison, L., Penny, W., 2003. Dynamic causal modelling. Neuroimage *19* (4), 1273–1302. https://doi.org/10.1016/s1053-8119(03)00202-7.

Gerchen, M.F., Bernal-Casas, D., Kirsch, P., 2014. Analyzing task-dependent brain network changes by whole-brain psychophysiological interactions: a comparison to conventional analysis. Hum. Brain Mapp. *35* (10), 5071–5082. https://doi.org/10.1002/hbm.22532.

Glasser, M.F., Sotiropoulos, S.N., Wilson, J.A., Coalson, T.S., Fischl, B., Andersson, J.L., Xu, J., Jbabdi, S., Webster, M., Polimeni, J.R., Van Essen, D.C., Jenkinson, M., Consortium, W.U.-M.H., 2013. The minimal preprocessing pipelines for the Human Connectome Project. Neuroimage *80*, 105–124. https://doi.org/10.1016/j.neuroimage.2013.04.127.

Gonzalez-Castillo, J., Kam, J.W.Y., Hoy, C.W., Bandettini, P.A., 2021. How to interpret resting-state fMRI: ask your participants. J. Neurosci. *41* (6), 1130–1141. https://doi.org/10.1523/Jneurosci.1786-20.2020.

Greene, A.S., Gao, S., Scheinost, D., Constable, R.T., 2018. Task-induced brain state manipulation improves prediction of individual traits. Nat. Commun. *9* (1), 2807. https://doi.org/10.1038/s41467-018-04920-3.

Hebb, D.O. (1949). The Organization of Behavior: A Neuropsychological Theory.

Honey, C.J., Sporns, O., Cammoun, L., Gigandet, X., Thiran, J.P., Meuli, R., Hagmann, P., 2009. Predicting human resting-state functional connectivity from structural connectivity. Proc. Natl. Acad. Sci. USA *106* (6), 2035–2040. https://doi.org/10.1073/pnas.0811168106.

Hutchison, R.M., Womelsdorf, T., Allen, E.A., Bandettini, P.A., Calhoun, V.D., Corbetta, M., Della Penna, S., Duyn, J.H., Glover, G.H., Gonzalez-Castillo, J., Handwerker, D.A., Keilholz, S., Kiviniemi, V., Leopold, D.A., de Pasquale, F., Sporns, O., Walter, M., Chang, C., 2013. Dynamic functional connectivity: promise, issues, and interpretations. Neuroimage *80*, 360–378. https://doi.org/10.1016/j.neuroimage.2013.05.079.

Iraji, A., Deramus, T.P., Lewis, N., Yaesoubi, M., Stephen, J.M., Erhardt, E., Belger, A., Ford, J.M., McEwen, S., Mathalon, D.H., Mueller, B.A., Pearlson, G.D., Potkin, S.G., Preda, A., Turner, J.A., Vaidya, J.G., van Erp, T.G.M., Calhoun, V.D., 2019. The spatial chronnectome reveals a dynamic interplay between functional segregation and integration. Hum. Brain Mapp. *40* (10), 3058–3077. https://doi.org/10.1002/hbm.24580.

Ji, G.J., Liao, W., Chen, F.F., Zhang, L., Wang, K., 2017. Low-frequency blood oxygen level-dependent fluctuations in the brain white matter: more than just noise. Sci. Bull. *62* (9), 656–657. https://doi.org/10.1016/j.scib.2017.03.021.

Ji, G.-J., Sun, J., Hua, Q., Zhang, L., Zhang, T., Bai, T., Wei, L., Wang, X., Qiu, B., Wang, A., Sun, H., Liao, W., Yu, F., Zhu, C., Tian, Y., He, K., Wang, K., 2023. White matter dysfunction in psychiatric disorders is associated with neurotransmitter and genetic profiles. Nat. Ment. Health *1* (9), 655–666. https://doi.org/10.1038/s44220-023-00111-2.

Jiang, R., Zuo, N., Ford, J.M., Qi, S., Zhi, D., Zhuo, C., Xu, Y., Fu, Z., Bustillo, J., Turner, J.A., Calhoun, V.D., Sui, J., 2020. Task-induced brain connectivity promotes the detection of individual differences in brain-behavior relationships. Neuroimage *207*, 116370. https://doi.org/10.1016/j.neuroimage.2019.116370.

Jiang, Y.C., Yao, D.Z., Zhou, J.Y., Tan, Y., Huang, H., Wang, M.L., Chang, X., Duan, M.J., Luo, C., 2022. Characteristics of disrupted topological organization in white matter functional connectome in schizophrenia. https://doi.org/Pii S0033291720003141 Psychol. Med. *52* (7), 1333–1343. https://doi.org/10.1017/S0033291720003141.

Kiviniemi, V., Vire, T., Remes, J., Elseoud, A.A., Starck, T., Tervonen, O., Nikkinen, J., 2011. A sliding time-window ICA reveals spatial variability of the default mode network in time. Brain Connect *1* (4), 339–347. https://doi.org/10.1089/brain.2011.0036.

Liu, J., Xia, M., Wang, X., Liao, X., He, Y., 2020. The spatial organization of the chronnectome associates with cortical hierarchy and transcriptional profiles in the human brain. Neuroimage *222*, 117296. https://doi.org/10.1016/j.neuroimage.2020.117296.

Liu, X., Chang, C., Duyn, J.H., 2013. Decomposition of spontaneous brain activity into distinct fMRI co-activation patterns. Front Syst. Neurosci. *7*, 101. https://doi.org/10.3389/fnsys.2013.00101.

Power, J.D., Barnes, K.A., Snyder, A.Z., Schlaggar, B.L., Petersen, S.E., 2012. Spurious but systematic correlations in functional connectivity MRI networks arise from subject motion (vol 59, pg 2142, 2012). -999 Neuroimage *63* (2), 999. https://doi.org/10.1016/j.neuroimage.2012.01.069.

Shine, J.M., Koyejo, O., Bell, P.T., Gorgolewski, K.J., Gilat, M., Poldrack, R.A., 2015. Estimation of dynamic functional connectivity using Multiplication of Temporal Derivatives. Neuroimage *122*, 399–407. https://doi.org/10.1016/j.neuroimage.2015.07.064.

Sivakolundu, D.K., West, K.L., Maruthy, G.B., Zuppichini, M., Turner, M.P., Abdelkarim, D., Zhao, Y.G., Nguyen, D., Spence, J.S., Lu, H.Z., Okuda, D.T., Rypma, B., 2020. Reduced arterial compliance along the cerebrovascular tree predicts cognitive slowing in multiple sclerosis: Evidence for a neurovascular uncoupling hypothesis. https://doi.org/Unsp 1352458519866605 Mult. Scler. J. *26* (12), 1486–1496. https://doi.org/10.1177/1352458519866605.

Smith, S.M., Miller, K.L., Salimi-Khorshidi, G., Webster, M., Beckmann, C.F., Nichols, T. E., Ramsey, J.D., Woolrich, M.W., 2011. Network modelling methods for FMRI. Neuroimage *54* (2), 875–891. https://doi.org/10.1016/j.neuroimage.2010.08.063.

Stephan, K.E., Penny, W.D., Moran, R.J., den Ouden, H.E., Daunizeau, J., Friston, K.J., 2010. Ten simple rules for dynamic causal modeling. Neuroimage *49* (4), 3099–3109. https://doi.org/10.1016/j.neuroimage.2009.11.015.

Van Essen, D.C., Ugurbil, K., Auerbach, E., Barch, D., Behrens, T.E., Bucholz, R., Chang, A., Chen, L., Corbetta, M., Curtiss, S.W., Della Penna, S., Feinberg, D., Glasser, M.F., Harel, N., Heath, A.C., Larson-Prior, L., Marcus, D., Michalareas, G., Moeller, S., Consortium, W.U.-M.H., 2012. The Human Connectome Project: a data acquisition perspective. Neuroimage *62* (4), 2222–2231. https://doi.org/10.1016/j.neuroimage.2012.02.018.

Wasserstein, R.L., Lazar, N.A., 2016. The ASA's Statement on -Values: Context, Process, and Purpose. Am. Stat. *70* (2), 129–131. <Go to ISI>://WOS:000378462300001.

Weissenbacher, A., Kasess, C., Gerstl, F., Lanzenberger, R., Moser, E., Windischberger, C., 2009. Correlations and anticorrelations in resting-state functional connectivity MRI: A quantitative comparison of preprocessing strategies. Neuroimage *47* (4), 1408–1416. https://doi.org/10.1016/j.neuroimage.2009.05.005.

Yeo, B.T.T., Krienen, F.M., Chee, M.W.L., Buckner, R.L., 2014. Estimates of segregation and overlap of functional connectivity networks in the human cerebral cortex. Neuroimage *88*, 212–227. https://doi.org/10.1016/j.neuroimage.2013.10.046.

Zhao, W.Q., Makowski, C., Hagler, D.J., Garavan, H.P., Thompson, W.K., Greene, D.J., Jernigan, T.L., Dale, A.M., 2023. Task fMRI paradigms may capture more behaviorally relevant information than resting-state functional connectivity. https://doi.org/ARTN 119946 Neuroimage *270*. https://doi.org/10.1016/j.neuroimage.2023.119946.